Journal of Applied Physics

Analog of electromagnetically induced transparency in metasurfaces composed of identical dielectric disks

Cite as: J. Appl. Phys. **129**, 063101 (2021); https://doi.org/10.1063/5.0036500
Submitted: 05 November 2020 . Accepted: 24 January 2021 . Published Online: 09 February 2021

Saeid Jamilan, George Semouchkin, and Elena Semouchkina

Journal of Applied Physics ARTICLE scitation.org/journal/jap

Analog of electromagnetically induced transparency in metasurfaces composed of identical dielectric disks

Cite as: J. Appl. Phys. **129**, 063101 (2021); doi: 10.1063/5.0036500
Submitted: 5 November 2020 · Accepted: 24 January 2021 ·
Published Online: 9 February 2021

Saeid Jamilan,[a] George Semouchkin, and Elena Semouchkina

AFFILIATIONS

Department of Electrical and Computer Engineering, Michigan Technological University, Houghton, Michigan 49931, USA

[a]**Author to whom correspondence should be addressed:** sjamilan@mtu.edu

ABSTRACT

An analog of electromagnetically induced transparency was revealed in metasurfaces (MSs), composed from identical dielectric resonators of simple cylindrical shapes. It was detected in numerical experiments at optical and microwave frequencies and confirmed by real experiments in the microwave range. The main specific of the observed phenomenon was its appearance at frequencies of electric dipolar resonances (EDRs) in MS elements, when total reflection of incident waves instead of transmission was expected. Investigations of electric field distributions in MSs allowed for detecting several Fano resonances caused by interaction between background radiation defined by incident waves, and radiation produced by oscillations of resonance fields in dielectric particles. The characteristics for EDR changes in phases of resonance oscillations by π radians were found controlling the transitions from constructive to destructive interference between participating wave processes. The onset of destructive interference was marked by sharp jumps by π radians in the spectra of signal phases. Performed analysis revealed that zero signals at Fano resonances, observed in the gaps between resonators, arranged along the electric field direction, could serve as indicators of realizing the conditions necessary for the transparency of MSs. These conditions included the elimination of the presence of background radiation and thus of interaction between trespassing waves and MSs.

I. INTRODUCTION

The phenomenon of induced transparency of otherwise opaque medium was initially revealed in atomic gases, where it was named "electromagnetically induced transparency" (EIT) and was considered as defined by destructive quantum interference between competing electron transitions, which led to the appearance of a narrowband window for the trespassing light.[1–3] Later, similar window openings at wavelengths far longer than those in atomic gases were observed in arrays of metallic meandered wires,[4] coupled plasmonic resonators,[5] as well as in metamaterials and metasurfaces (MSs), composed of specially designed resonators including dielectric ones.[6–10] All these structures were found capable of supporting full propagation of incident electromagnetic waves within a narrow band, while at lower or higher frequencies, waves were either completely reflected or absorbed. The fact that phenomenologically similar results were obtained in quite different substances did not seem surprising since it was shown in Ref. 11 that basic characteristics of EIT-like phenomena in quantum gases could be modeled by using classical systems of coupled harmonic oscillators (coupled RLC circuits in electrical models or properly connected particles and springs in mechanical models).

Different from the above referenced works on metamaterials and MSs composed of resonators with a complex configuration, we observed narrowband transparency at electric dipolar resonances in densely packed MSs formed from simple silicon resonators of cylindrical or disk shapes.[12,13] At such MS geometries, the concept of interfering bright and dark modes in coupled resonators, which was conventionally used for explaining EIT-like phenomena in multi-resonator arrays, could not be applied. In this work, we present the results of investigations, which allow for forwarding an alternative concept, clarifying the reasons for induced transparency of MSs composed of identical disk resonators. In particular, we pay special attention to Fano-type resonances in MSs under study. These resonances, as known, are the product of interference between competing wave processes.[6,14,15] A deeper insight into the formation of Fano resonances in MSs allows us to understand wave

processes, which define the appearance of the EIT-type phenomenon in MSs under study.

It should be noted here that employing the EIT phenomena promises significant advances in optical information processing. In particular, opening a narrowband transparency window at EIT was found to result in a dramatic reduction of the light group velocity, i.e., in slow light,[16] enabling even complete stop of the propagating optical pulse and its storage in the atomic ensembles.[17] Similar stop was observed in waveguides, side-coupled to tunable resonators, when a photonic band structure representing a classical analog of EIT was generated.[18] Slow light was also used in optical networks for implementing optical buffers.[19] Tunable optical buffers were recently developed by using an analog of EIT in coupled photonic crystal cavities.[20] In Ref. 21, the EIT was used to build optical switches and wavelength converters. In Ref. 22, it was proposed to design switches and filters by using switchable EIT phenomenon in graphene-loaded MSs composed of split silicon nano-cuboids. Thus, it is expected that realizing EIT in very simple MSs will open up additional perspectives for various applications.

II. MODEL AND METHOD DESCRIPTION

Figure 1 presents the schematic of MS fragments used in our studies. The structures were composed of silicon cylinders or disks with the diameters (D) of 240 nm and heights (h) varied from 100 nm to 240 nm. These cylinders/disks are further called "dielectric resonators" (DRs). Parameters of resonators were chosen to provide comparison of obtained results with the results of our earlier studies,[12,23,24] as well as with the data, presented in well-known works on silicon MSs.[25,26] Lattice parameters (Δ) of MSs under study were varied in the range from 275 nm to 450 nm. At a smaller Δ, the structures were considered as densely packed, since the distances between DRs in such structures could be equal to 35 nm, that was much smaller than the diameters of silicon particles, while at a larger Δ, the structures were considered as rather sparsely packed, since the distances between DRs approached 210 nm, i.e., became compared to the diameters of DRs. The terms "dense" and "sparse" were introduced earlier in Refs. 12, 23, and 24, to stress out significant differences in responses of MS structures with different Δ's.

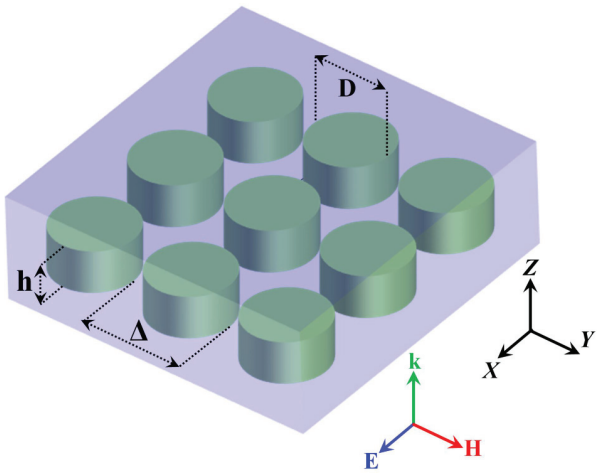

FIG. 1. Schematic of MSs composed of silicon nano-disks.

The studies were conducted for MSs with square and rectangular lattices. To verify the results of numerical experiments, we compared the data obtained by using two types of commercial software: COMSOL Multiphysics and CST Microwave Studio. As seen in Fig. 1, incident waves were sent normally to MS planes with electric (E) and magnetic (H) field vectors, directed along x and y axes, respectively. The amplitude of incident wave's electric component was always fixed at 1 V/m. Field data and scattering parameters (S-parameters) were directly extracted from the results of simulations. In simulation models, DRs were placed in air that allowed for investigating the basic physics of MS performance without complications arising from substrate involvement. It is, however, shown in Sec. III that inserting substrates did not deteriorate observed EIT-type effects.

As it was demonstrated in our earlier work,[24] all characteristic features of MS responses could be conserved, when the structures with nano-sized particles, used in the optical range, are rescaled for operating in the microwave range, where experimental studies are much easier to perform. Therefore, in this work, experiments were performed at microwave frequencies with MSs, composed of ceramic mm-size resonators. Parameters of resonators and MSs were chosen to provide scaling of the phenomenon of induced transparency from the optical to microwave range. The experimental technique is described in Sec. IV.

III. DETECTING THE TRANSPARENCY OF DENSELY PACKED MSs

The phenomenon of induced transparency in densely packed MSs with square lattices, composed of cylindrical silicon resonators, was first noticed in Ref. 12 at the studies of MS resonance responses in dependence on DR heights. In these studies, the lattice constant of MSs was kept on the level of 300 nm, while changes of MS responses were provided by varying the heights of constituent resonators in the range from 200 nm to 100 nm. In particular, the spectra of electric (E) and magnetic (H) field probe signals and transmission spectra S21 were investigated. The effects, reminding the EIT phenomenon, were detected in the spectra of S-parameters, which demonstrated sharp peaks of S21 up to 1 and narrowband drops of S11 down to zero at the frequencies of electric dipolar resonances (EDRs).

Figure 2 demonstrates EIT-like responses, simulated by using either COMSOL or CST software, for MSs with DRs placed either in air or on the PDMS substrate with relative permittivity of 2.25 and thickness of 200 nm. The observed S-parameter spectra narrow transparency window is surprising, since the formation of Mie resonances in dielectric MSs is usually associated with spectral regions of high reflections.

Figure 3 presents S-parameter spectra of MSs with square lattices and the spectra of E- and H-probe signals, obtained at placing the probes in the centers of DRs, at different lattice constants of MSs. Since the properties of MSs could be also modified by

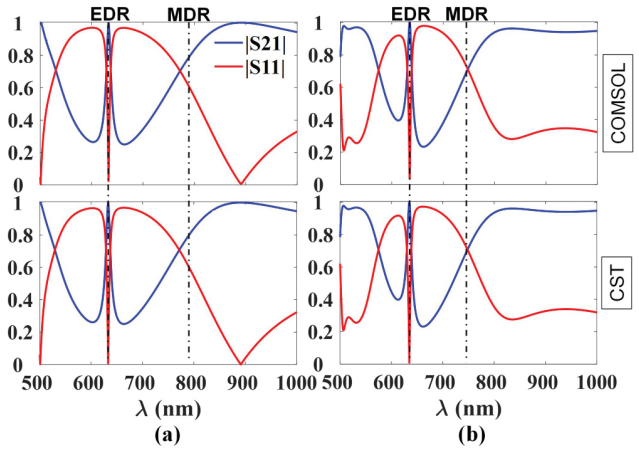

FIG. 2. S-parameters spectra for MSs with square lattices and lattice constants of 275 nm, simulated by using COMSOL (upper row) and CST (lower row) software. Heights of silicon disks were 160 nm, while they were placed in (a) air and (b) on the PDMS substrate with a thickness of 200 nm. Diameters of DRs were 240 nm. Spectral positions of EDRs and magnetic dipolar resonances (MDRs) are indicated by vertical dashed-dotted lines.

changing the DR heights, Fig. 3 allows for comparing the data, obtained for MSs with DR heights of 160 nm and 130 nm.

As seen in the figure, S-parameter spectra in most dense MSs (at $\Delta < 300$ nm) exhibit the features, which are very common for multiple demonstrations of EIT in the literature.[4–10] In particular, narrowband peaks of S21, combined with sharp dips of S11, are seen in the surrounding of gradually varying parts of two spectra, which are less or more symmetric with respect to EIT windows. For MSs with $\Delta < 325$ nm, no other singularities of S parameters could be found in spectral regions near EDRs, i.e., nothing disturbed the opaque property of MSs, except for peaks of S21 at deep drops of S11 at EDR frequencies.

Most symmetric with respect to EDRs' EIT-type responses were observed in MSs with $h = 160$ nm at the lattice constant $\Delta = 275$ nm and in MSs with $h = 130$ nm at the lattice constant $\Delta = 300$ nm. At increasing Δ, combined S21 peaks and S11 dips continued to be seen in S-parameter spectra of MSs at all values of Δ up to 400 nm. However, the symmetry of S-parameter spectra on the blue and red sides of the EIT-type singularity disappeared for the case $h = 160$ nm at $\Delta > 300$ nm. Gradually, the two spectra, S21 and S11, became anti-symmetric in the EIT area. In particular, in addition to initial peaks of S21, accompanied by S11 dips, a wide ridge of close to unity S11 values, accompanied by dips of S21,

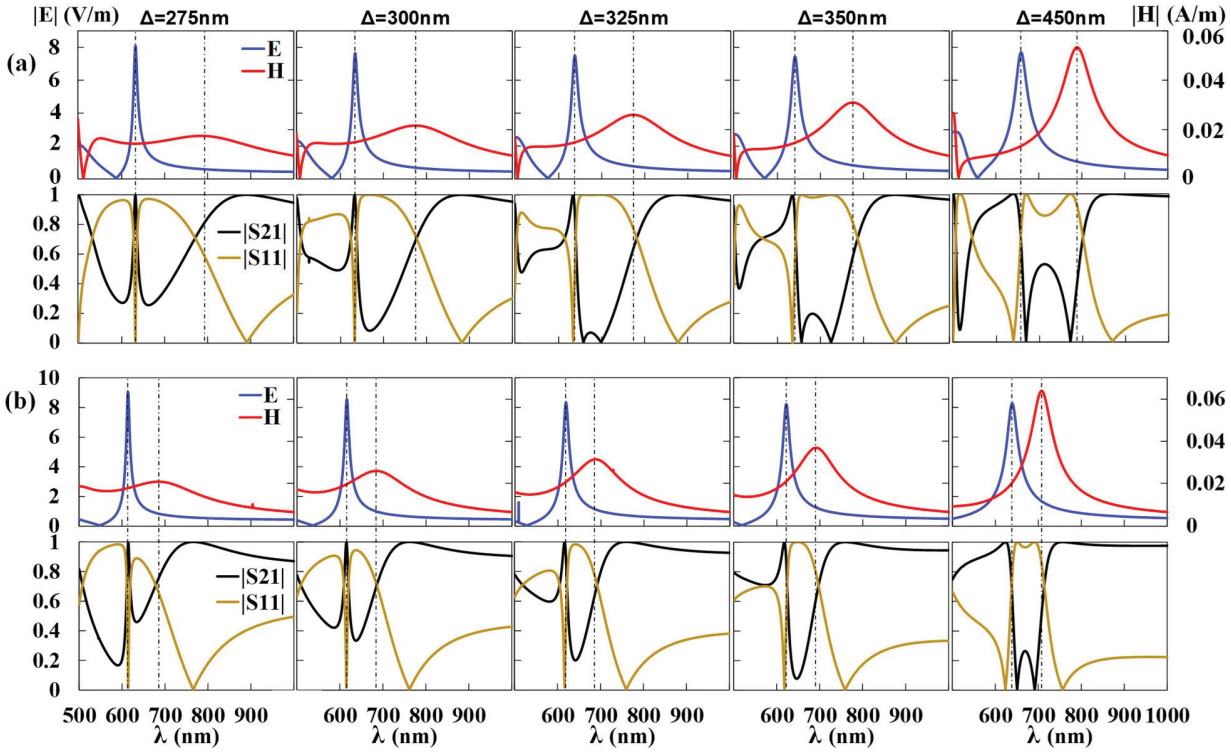

FIG. 3. E- and H-field probe signal spectra and S-parameter spectra at various lattice constants of silicon MSs with square lattices, having different heights of constituent resonators: (a) 160 nm and (b) 130 nm. Diameters of resonators are 240 nm.

appeared at slightly longer wavelengths. At $\Delta = 325$ nm and above, two spectra crossed each other at wavelengths between the spectral locations of their extrema. As known, similar crossings were noticed in S-parameter spectra of dipole antennas (when $|S21| = |S11| = 0.7$). At lattice constants of about 450 nm, sharp S21 peaks could not be seen anymore, but the tops of wide S21 ridges, formed instead of peaks, still approached the unity value at some wavelength λ, smaller than λ_{EDR}, while S11 continued to demonstrate dips down to zero. It is worth noting here that the described above changes occurred along with the appearance of deep depression of S21 on the red side of EIT-type window at $\Delta > 300$ nm [that is especially well seen in Fig. 3(a)]. At further increasing Δ, this depression transformed into dual dips of S21, usually associated in sparse structures with two dipolar resonances (electric and magnetic ones), which were expected to cause zero transmission at total reflection. However, such a direct association is not obvious from the data presented in Fig. 3, especially for magnetic resonance, since it appeared in probe signal spectra at longer wavelengths than wavelengths of red-side S21 dips. Positions of S21 dips, located at shorter wavelengths, experienced relatively small spectral changes at increasing the Δ values, but at bigger Δ, they approached the positions of electric resonances, since the latter shifted to the red side of the spectra. Altogether, the described changes, observed at increasing Δ, transformed S-parameter spectra into configurations, which were characteristic for sparse MSs.[12]

From the comparison of sets (a) and (b) in Fig. 3, it could be noticed that decreasing DR heights allows for shifting EIT window to shorter wavelengths, as well as for increasing the range of lattice constants, at which typical for EIT features of S-parameter spectra could be observed. However, at $\Delta = 450$ nm, the spectra of MSs with DRs of different heights acquired similar shapes.

It is also seen in Fig. 3 that at wavelengths longer than those, corresponding to positions of red-side dips in S21 spectra and positions of MDRs in probe signal spectra, S-parameter spectra of MSs demonstrate one more singularity, i.e., regions with full transmission ($|S21| = 1$) and sharp drops of reflection coefficient S11 down to zero. This phenomenon is characteristic for Kerker's effect, which is observed at interference between waves, radiated by oscillating fields of electric and magnetic resonances in MS particles. The results of our studies of this effect in MSs, composed of silicon nano-disks, were presented in our earlier work.[12]

Figure 4 provides color-scaled (3D) representations of the discussed above transformations of S-parameter spectra at increasing the lattice constants, which help to understand the factors, restricting the realization of induced transparency in MSs composed of silicon disks. It is well seen in the figure that in dense structures with $\Delta < 325$ nm, the EIT-like phenomenon reveals itself in S21 spectra as a spectrally narrow strip of red color, which corresponds to full transmission ($|S21| = 1$). In S11 spectra, induced transparency causes appearance of a narrow strip of dark-blue color, which corresponds to zero reflection ($|S11| = 0$). At increasing the Δ values, both strips become wider. However, the EIT-related strip in the image of S21 spectra becomes several times wider, when Δ changes from 325 nm to 375 nm, while a similar strip in the image of S11 spectra remains relatively narrow at increasing Δ up to 450 nm.

Figure 4 also visualizes the deterioration of the symmetry of S-parameter spectra at bigger lattice constants. As seen in the image of S21 spectra, the EIT-related strip crosses identically colored light blue areas only at $\Delta < 325$ nm, while at bigger Δ, the colors on two sides of the strip become contrast: red color marks close to unity values of S21, while blue color marks close to zero values of S21 that excludes any symmetry. The EIT-related strip in the image of S11 spectra passes between two identically colored red areas (with $|S11| = 1$) only at $\Delta < 325$ nm, while at bigger Δ, the area to the left from the strip becomes colored light blue, while the area to the right turns to become dark red (with $|S11| = 1$) that also excludes any symmetry in S11 spectra.

In addition to deteriorating the symmetry of S-parameter spectra at increasing the array lattice constant, there is another reason, which restricts realizing EIT-type effects in sparse MSs. As it is seen from the presented data, the Q-factors of observed phenomena in MSs with bigger lattice constants look significantly decreased. In the literature related to the EIT phenomenon, high

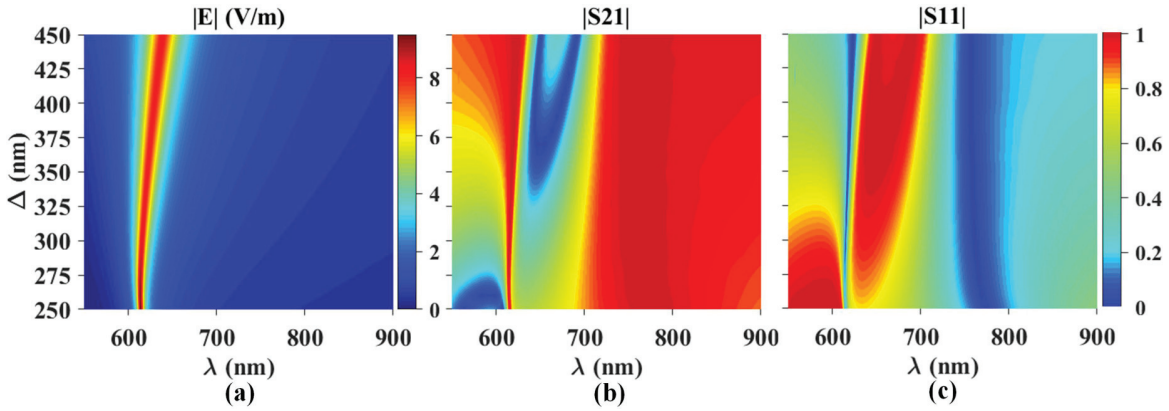

FIG. 4. Effects of MS periodicity on (a) spectral positions of EDRs and on color-scaled images of (b) S21 and (c) S11 spectra. DR heights in all MSs were kept equal to 130 nm, diameters of DR were 240 nm.

Q-factors are considered as an important benefit, degrading of which can create problems for obtaining practically important slow-light effects. Therefore, it was desirable to look for opportunities to increase the range of options for realizing narrow band of EIT in MSs. For this purpose, we investigated the EIT-type phenomena in MSs with rectangular lattices. In these studies, we fixed the "dense" value of Δ (275 nm) in either X- or Y-direction, while varied the Δ value for another direction in a wide range.

Figure 5(a) shows, how S-parameter spectra change at extending lattice cells of MSs in the X-direction, while the Δy value is fixed. As seen in the figure, these changes have a lot in common with changes observed in Fig. 3(a) for MSs with square lattices. In particular, there is a similar difference in the changes of S-parameters in blue and red parts of the spectra around the EIT singularity, and similar appearance of anti-symmetric lineshapes in S21 and S11 spectra, with their crossings at close to EDR wavelengths at bigger Δ. The only difference of the case with rectangular lattices vs the case with square lattices is seen in very sharp, almost vertical, drops of S11 near EDRs and in conserved peaking of S21 curves at EDRs even at Δy = 525 nm. The similarity of the basic features of the data presented in Figs. 3(a) and 5(a) (both sets were obtained at DR heights of 160 nm) implies that these features are controlled by changing the Δx values, regardless of whether these changes are accompanied by similar changes of Δy, or Δy remains fixed at the value of 275 nm.

However, extending lattice cells of MSs in the Y-direction at keeping Δx fixed at the level, characteristic for dense structures, does not produce changes in S-parameter spectra, comparable to those, observed at extending lattice cells in the X-direction. As seen in Fig. 5(b), S-parameter spectra conserve such characteristic features of EIT, as full transmission and zero reflections at EDR wavelengths, at increasing Δy up to 450 nm and even bigger values. However, the lineshapes of S11 and S21 spectra degrade at increasing Δy, in comparison with the lineshapes observed for MSs with square lattices at Δ = 275 nm. In particular, the peaks and dips of S-parameters become essentially less sharp and are characterized by much smaller Q-factors, compared to narrowband EIT-like singularities. At Δy = 500 nm and bigger, EDRs reveal themselves in S-parameter spectra by wide dips of S11 down to zero, comparable to dips observed at Kerker's conditions, and by hill-like patterns of S21 spectra at the frequencies of EDRs. It is also worth noting that increasing Δy practically does not change spectral positions of MDRs, while the positions of EDRs demonstrate red shifts, thus bringing two resonances closer to each other. The specifics of

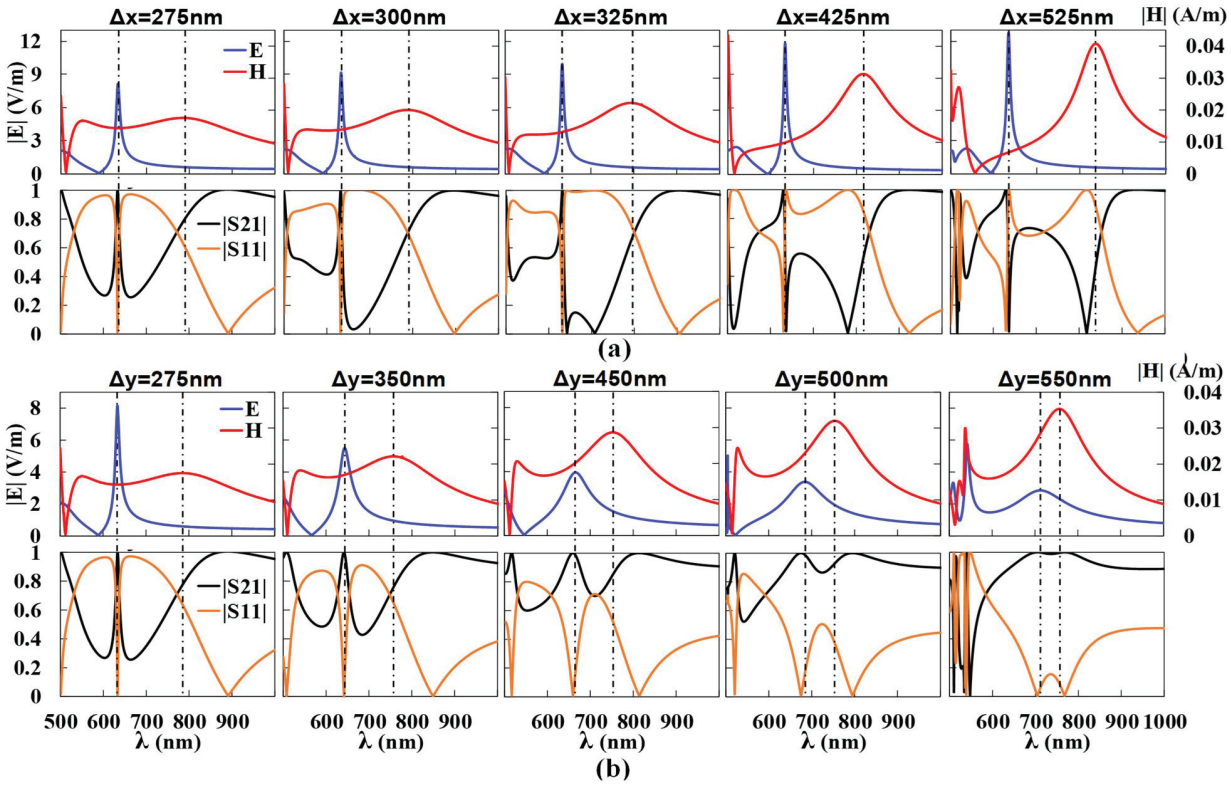

FIG. 5. Transformations of E- and H-field probe signal spectra and S-parameter spectra at modifying MSs by extending their unit cells: (a) along the x axis at fixed Δy = 275 nm, and (b) along the y axis at fixed Δx = 275 nm. Vertical dashed-dotted lines show spectral positions of EDRs and MDRs. DR heights in all MSs are 160 nm, while DR diameters are 240 nm.

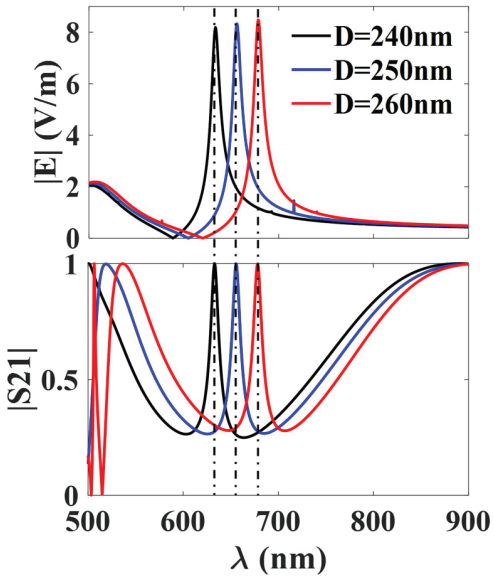

FIG. 6. Simulated responses of dense MSs composed of silicon disks with identical heights of 160 nm and various diameters. DR diameters are, respectively, 240, 250, and 260 nm, and lattice constants of respective MSs are 275, 287, and 301 nm, respectively.

changes in S-parameter spectra at extending lattice cells in the Y-direction allows for suggesting that, in difference from extending the cells in the X-direction, such lattice transformation does not deteriorate physical processes, responsible for the EIT phenomenon, while provides more options for its realization. It is worth noting that significant red shifting of EDR's spectral positions at $\Delta y > 450$ nm is apparently caused by the formation of lattice resonances, when Δy approaches the values corresponding to the appearance of Rayleigh anomalies.[27] This shift, however, does not occur in densely packed MSs.

EIT wavelength could be changed by changing EDR frequency at varying aspect ratio of DRs. In Figs. 3(a) and 3(b), heights of disks were changed, while their diameters were fixed equal to 240 nm. Figure 6 shows that an increase of DR diameters from 240 nm up to 260 nm, if DR heights are fixed equal to 160 nm and lattice constants Δ are properly adjusted, leads to red shifting EIT wavelengths. This could be used for adjusting the spectral position of EIT windows in dense MSs composed of identical dielectric disks.

IV. SCALING MSs AND EXPERIMENTAL CONFIRMATION OF INDUCED TRANSPARENCY IN THE MICROWAVE RANGE

To scale MSs for performing microwave experiments, we followed the approach used in Ref. 24. Similar to optical nanoresonators, microwave resonators were initially supposed to have relative permittivity of 12.25. Resonators were represented by disks with the diameters of 6 mm and the heights of 3.5 mm. To provide desirable MS responses, lattice constants were chosen in the range from 6.5 mm to 12 mm. As seen in Fig. 7, using the above listed parameters allowed for reproducing in S-parameter spectra of "microwave" MSs all details, characteristic for S-parameter spectra of MSs, composed of nano-resonators.

As seen in the figure, the EIT-type peak of S21 parameter, combined with the dip down to zero of S11 parameter, was obtained for microwave MSs at the frequency of electric dipolar resonance. Similar to the case of optical MSs, this singularity in S-parameter spectra of microwave MSs were accompanied by the enhancement of reflections on both sides of S21 peak that allowed for describing the phenomenon as appearance of a narrowband transparency window for incident waves in otherwise opaque medium. Similar to the optical case, S-parameter spectra of microwave MS demonstrated crossing of S21 and S11 spectra at the frequency, close to the frequency of magnetic dipolar resonance, and also the features, characteristic for Kerker's effect (at f = 20 GHz).[12,24]

Since the frequency, corresponding to the S21 peak in the spectrum of microwave MS appeared to be higher, than that convenient for experiments, the permittivity of DRs had to be increased. The results of simulations, presented in Fig. 8, show, how the frequency range, necessary for the observation of induced transparency in microwave MSs, changes at varying the values of dielectric permittivity of the resonator material.

As seen in Fig. 8, the desired frequency range, centered around 11 GHz, is achievable in MSs, composed of resonators with the relative permittivity close to 40, instead of 12.25. Presented in Fig. 8 data also show that increasing the permittivity of dielectric material improves the shape of the singularity, representing the induced transparency, i.e., the Q factor of related S21 peaks. In addition, MSs' responses on both sides of the singularity demonstrate strongly opaque properties of the medium. Based on the obtained data, arrays of ceramic resonators with the diameters and

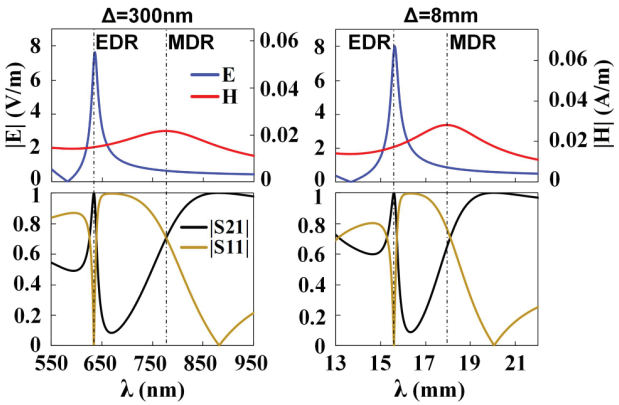

FIG. 7. Upper row: simulated E- and H-field signals from probes located in centers of MS resonators. Lower row: simulated S-parameter spectra of MSs. Left column: optical MSs with a lattice constant of 300 nm, composed of DRs with h = 160 nm, D = 240 nm, $\varepsilon = 12.25$. Right column: microwave MSs with a lattice constant of 8 mm, composed of DRs with h = 3.5 mm, D = 6 mm, $\varepsilon = 12.25$.

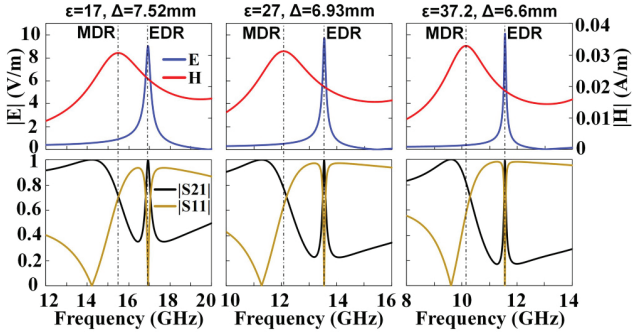

FIG. 8. Upper row: simulated E- and H-field signals from probes located in centers of MS resonators. Lower row: simulated S-parameter spectra for densely packed MSs, composed of DRs with h = 3 mm, D = 6 mm. The relative permittivity of DRs in three MSs, from left to right, is equal to 17, 27, and 37.2, respectively.

heights of, respectively, 6 mm and 3 mm, and the relative permittivity of 37.2, have been selected for microwave experiments.

Figure 9 shows the schematic of experimental setup with the MS sample. The samples were representing arrays of disk resonators with square lattices of various lattice constants. Arrays were fixed on paper boards by using double-sided sticky tape. As seen in Fig. 8, the MS sample was placed between two identical X-band horn antennas (with operating frequencies from 8 GHz to 12 GHz),

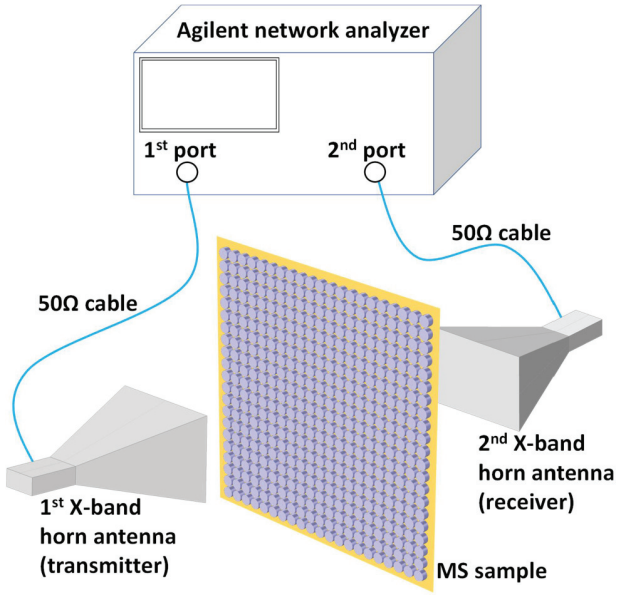

FIG. 9. Schematic of experimental setup with the vector network analyzer, two X-band horn antennas, operating in the range of 8 GHz–12 GHz, 50 Ω coaxial cables, and MS sample.

transmitting and receiving ones. Horn antennas were connected by standard 50 Ω coaxial cables to an Agilent vector network analyzer with the frequency range of 10 MHz–20 GHz.

The responses of four MS samples with different lattice constants are presented in Fig. 10. As seen in the figure, simulated and experimental spectra of S-parameters demonstrated good agreement. In particular, at Δ = 8 mm, both spectra showed dual dips of S21 on the red side of the small peak with full transmission. This peak was located at about 11.6 GHz, i.e., very close to the frequency of electric dipolar resonance, detected in the probe signal spectrum in Fig. 8, while dual dips, associated with reflections from dipolar resonances, were related to magnetic response at about 11 GHz and to electric response at the frequency, close to 11.5 GHz. It should be noted that in our earlier works[12,24] we observed appearance of related to dipolar resonances dual dips of S21 in relatively sparse MSs, composed of nano-resonators. These dips were related to conventional reflections from resonating nano-elements. As seen in Fig. 10, at decreasing the lattice constant to Δ = 7.3 mm, two dips in simulated spectra came closer to each other and at Δ = 7 mm, they merged in one dip. At decreasing the lattice constant down to Δ = 6.6 mm, the S21 spectrum acquired the shape, quite similar to that of a typical EIT-type spectrum, with a narrow peak of full transmission, located between symmetrical spectral parts with very low, opaque-type transmission. From the experimental S21 spectrum, obtained at Δ = 6.6 mm, it is not obvious that the spectral location of the peak with full transmission coincides with the position of electric dipolar resonance. However, comparison with the simulated probe signal spectrum, presented in Fig. 8 for MS with Δ = 6.6 mm, confirms this fact.

Conducted experiments with microwave MSs have confirmed that the phenomenon of induced transparency, revealed originally by simulations for MSs, composed of silicon nano-resonators, can be also realized in dense MSs, composed of ceramic microwave resonators.

V. ANALYSIS OF ELECTRIC FIELD DISTRIBUTIONS AND SEARCH FOR INTERFERENCE PARTNERS AT FANO RESONANCES

It is presumed that EIT is caused by interference between light-controlled processes, which are defined either by the specifics of excitation paths, as it is the case in atomic gases,[1–3] or by the specifics of overlapping electromagnetic fields in arrays of coupled resonators, when excitation is provided by only one source, such as plane wave.[4,6] In the case of MSs, composed from resonators of only one type, the concept of coupling between resonators of various types, responsible for the formation of either dark, or bright modes, does not seem adequate. In the literature, the bright mode typically refers to a resonance, directly excited by incident radiation in one type of resonators of the EIT system. The dark mode is a secondary resonance in another type of resonators, excited by the bright mode through coupling effects. It is usually assumed that destructive interactions between bright and dark modes can induce the transparency of multi-resonator EIT systems.

In order to explain appearance of induced transparency in MSs, composed of identical resonators, we had to look for alternative partners of interference. With this purpose, we analyzed

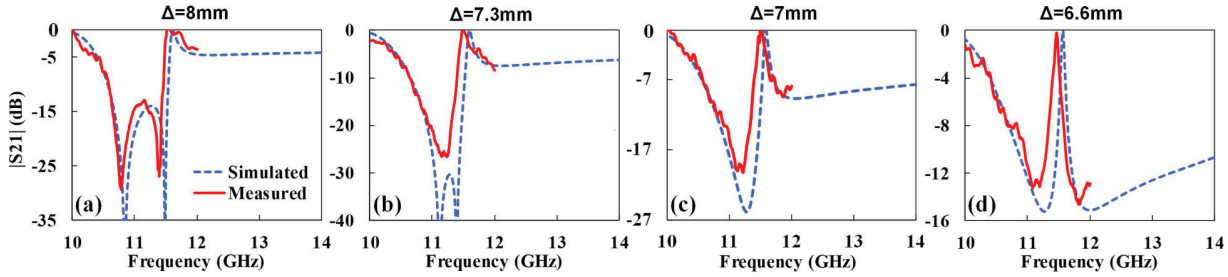

FIG. 10. Measured and simulated |S21| spectra (in dB) for MSs, composed of dielectric disks with the diameters and the heights of, respectively, 6 mm and 3 mm and relative permittivity of 37.2 at four various lattice constants ranging from 8 mm to 6.6 mm.

Fano-type responses, observed at the studies of dipolar resonances in MSs. These responses often demonstrated zeros of the signals, characteristic for Fano resonances. As known, such zeros could be considered as the product of destructive interference, which, in the case of Fano resonances, is usually expected between wideband background/incident radiation and narrowband resonance scattering.[6,14] To obtain more information about interference parties, we investigated Fano-type responses at some specific locations in MSs. Our previous studies of field distributions in planar cross sections of MSs[12,23,24] have shown that in dense structures with square lattices useful information could be provided not only by the resonance fields inside DRs, but also by the fields, formed in the gaps between resonators in the X- and Y-oriented rows of DRs, as well as by the fields in the centers of geometric cells.

Figure 11 exemplifies electric field patterns, observed in the planar XY cross section of the geometric cell of MSs with a square lattice at the frequency of EDRs. It is well seen that resonating

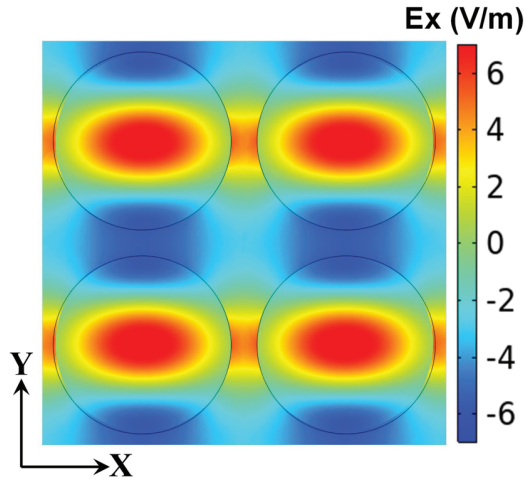

FIG. 11. E-field distribution in central planar cross section of a square-latticed MS at the wavelength of EDR's peak ($\lambda = 634$ nm). The heights and diameters of resonators are, respectively, 160 and 240 nm. The lattice constant is 275 nm.

dipoles are confined within DRs and provide strongest fields in DR centers. Electric fields in the gaps between resonators, arranged along the X direction, with which dipolar electric fields are co-directed, look uniformly distributed within the gaps, even at increasing the lattice constant. This means that resonance fields do not fully control fields in the gaps. As it was found in numerical experiments, at bigger lattice constants, the strengths of gap fields could decrease, when the strengths of dipolar fields demonstrated almost no changes. It allows for suggesting that fields, seen in X-oriented gaps between DRs, include contributions from incident waves, which interfere with dipolar fields. In such cases, these contributions from incident waves can be considered as background fields.

Although electric fields in the gaps between resonators, arranged along the Y direction, look directed oppositely to dipolar fields formed inside the resonators, they are apparently defined by field lines, originating from dipoles and passing in air around the resonators.[23] The strength of these fields in each of Y-oriented gaps is the result of combining field lines, coming from dipoles formed in neighboring resonators arranged along the Y direction. Therefore, the strength of these fields can be a measure of coupling between resonators.

Another specific feature of the field pattern in Fig. 11 is seen in relatively weak blue colored fields in the centers of MS geometric cells. These fields are co-directed with the fields in Y-oriented gaps, i.e., are opposite to dipolar fields formed inside resonators. However, they do not seem to be of the same origin, as that of the gap fields. At bigger lattice constants, these fields were found to strengthen and to contribute to the formation of specific field distributions, represented by parallel X-oriented field lines of alternating polarity and lattice-defined periodicity. Such types of distributions could be related to the formation of standing surface waves.

The presented analysis shows that field patterns, similar to that given in Fig. 11, integrate electric fields of different origins. The studies of these fields should be helpful for deeper insight into the physics of wave processes in MSs.

Figure 12 uses the schematic of one geometric cell of MSs with a square lattice to show the positions, which were chosen for placing E-field probes. Point P1, located in the center of DR, is used for characterizing the formation of dipolar resonances (EDRs). Point P2, placed in the middle of the gap between resonators arranged along the X direction, can describe interstitial fields

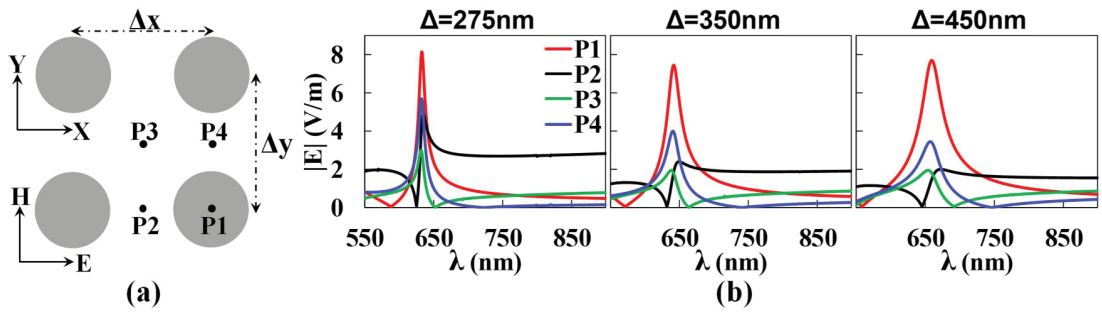

FIG. 12. (a) Geometric schematic of MS lattice cell with four points, chosen for placing E-field probes in planar MS cross section; (b) spectra of signals from E-field probes, placed according to the schematic shown in (a) in MSs with different lattice constants Δ. Resonator heights are 160 nm, and their diameters are 240 nm.

in X-oriented rows of DRs. Point P3 is used for judging about the surface wave contribution in field distributions. Point P4 is employed to characterize interstitial fields in Y-oriented rows of resonators.

As seen in Fig. 12, the spectra of signals from all probes in MSs with different lattice constants demonstrate features, typical for Fano-type resonances, and resonance maxima look located close to the wavelengths, characteristic for spectral positions of EDRs. In points P1, P3, and P4, beyond the spectral region defined by EDR-related phenomena, probe signals do not demonstrate any specific features, except for decaying, while in point P2, on the contrary, probe signals conserve significant strengths and remain stable in wide spectral ranges from 700 nm to 900 nm and above. The intensity of these stable signals is maximal in densest structures, while it decreases significantly in MSs with bigger lattice constants. The observed specifics of P2 signals justify the suggestion that they originate from incident waves, while their stable values in air-filled interstitials can be defined by incident fields distributed in a non-uniform air-dielectric medium. At increasing the Δ values, the voltage associated with incident fields has to be applied to sparser rows of resonators with wider air gaps that explains decreasing the field magnitudes in air gaps. This consideration is in favor of earlier made suggestion that the fields in X-oriented gaps can represent background fields, required for the formation of Fano-type responses.

VI. FANO RESONANCES AND INTERFERENCE PROCESSES

To analyze Fano resonances, revealed by signals from four E-field probes, we consider presented in Fig. 13 spectra of probe signal magnitudes and phases, along with the field patterns, observed at zero signals of respective Fano lineshapes. The data

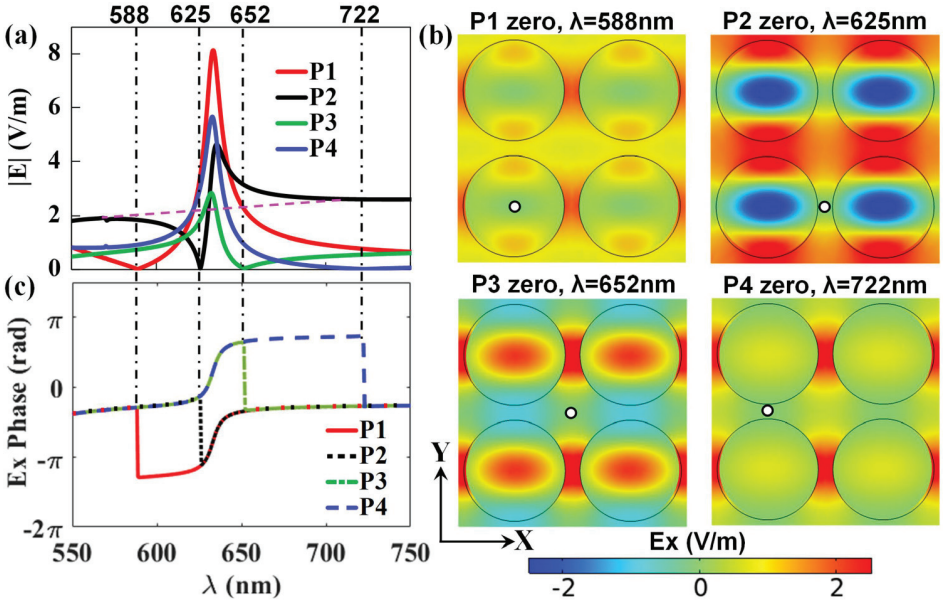

FIG. 13. (a) Spectra of E-field probe signals in four points of the MS geometric cell [see Fig. 12(a)]; (b) field patterns in planar cross sections of MS at wavelengths of zero signals in lineshapes of Fano resonances [see (a)]; and (c) spectra of probe signal phases in four points. Circles in field patterns exemplify zero field locations. MS lattice constants are equal to 275 nm, DR heights are 160 nm, and DR diameters are 240 nm. Dashed purple line in (a) shows the extension of the background portion of P2 signals.

presented in Fig. 13 were obtained for the dense MS with the lattice constant of 275 nm.

We start from analyzing the spectra of probe signals and field patterns, to draw first conclusions about interference processes in MSs under study, and then employ the spectra of probe signal phases for providing deeper insight. As seen in Fig. 13(a), the probe signal spectrum, obtained at point P1, demonstrates typical for EDR resonance peak at 634 nm with characteristic for Fano-type resonance zero signal in the lineshape at 588 nm, i.e., far from the peak. Since the strength of EDR fields at 588 nm is significantly decreased, it can be expected that the background radiation, destructive interference of which with resonance fields causes zero in the lineshape of P1 signal, is also weak. The data presented in Fig. 13(b) do not contradict these expectations, despite seemingly strong background fields in air-filled interstitials of X-oriented rows of DRs at 588 nm. In fact, the strength of background fields inside DRs, where they compete with resonance fields, should be much smaller than it is in air, since the value of DR's dielectric constant is equal to 12.25.

The spectrum registered at point P4, which should characterize dipolar fields, circling around resonators, also demonstrates a peak at the EDR wavelength of 634 nm. However, the respective Fano-type lineshape at point P4 has its zero in the red portion of the spectrum, i.e., at 722 nm that agrees with the opposite polarity of fields in Y-oriented gaps, with respect to the polarity of dipolar fields inside resonators. The spectrum of P2 signal reveals classic Fano-type lineshape in the vicinity of EDR. It is characterized by a peak on the red side of EDR and by a deep drop down to zero on the blue side of EDR. These features allow for suggesting that Fano resonance in point P2 is defined by interference of background radiation and signals, radiated by EDRs. At $\lambda = 625$ nm, corresponding to the location of zero in the Fano lineshape at point P2, the respective field pattern in Fig. 13(b) demonstrates zero fields in X-oriented gaps that tells about total suppression of background/incident radiation in these gaps by the fields, radiated from resonating dipoles. Destructive interference of two fields is the result of their π-value phase difference, which will be confirmed below at the analysis of phase changes given in Fig. 13(c).

It should be accentuated here that competing wave processes, which define the appearance of Fano resonances, should be in phase at constructive interference and should be shifted by π radians at destructive interference. Therefore, if one of two processes does not change the phase in the spectral range, corresponding to the transition from constructive to destructive interference at Fano resonance, then the second process must experience phase shift by π radians in the same spectral range. In the case under consideration, the formation of dipolar resonances should be accompanied by changes of the phase of resonance oscillations by π in the spectral range between red and blue ends of the resonance lineshape. This knowledge should be kept in mind at the analysis of phase changes, which probe signals experience at the formation of Fano responses in the chosen four points of MSs.

As seen in Fig. 13(c), the spectra of probe signal phases at Fano resonances in all four points of MS cross section, experience at least one jump up by π radians at moving along the spectra from longer to shorter wavelengths. However, spectral positions of these jumps are specific for probe locations, since jumps occur at the wavelengths, corresponding to zeros in the lineshapes of respective Fano resonances.

In addition to sharp jumps, all spectra of probe signal phases demonstrate gradual decrease of signal phases by π radians in the range of wavelengths, corresponding to the EDR region in P1 spectrum. This decrease is apparently due to switching of the phase of resonance oscillations by π radians at dipolar resonances. The fact, that similar changes are observed in P2, P3, and P4 spectra, indicates that they are controlled by EDR-caused radiation. In difference from gradual changes, sharp jumps by π radians in the spectra of probe signal phases indicate that at zero signals in Fano lineshapes, defined by destructive interference of competing wave processes, there is a change of the leader in this competition.

Clarification of the nature of competing wave processes can be exemplified by the case of P2 signal. It is seen in Fig. 13(c) that, while the phase of P2 signal coincides with the phase of P1 signal in the range $750\ \text{nm} > \lambda > 625$ nm, the phases of two signals become different by π radians after the π-value jump up of P2 phase at $\lambda = 625$ nm. Sin-phase changes of P1 and P2 signals in the red portion of EDR-related spectral range indicate that in this spectral portion, P2 signal is controlled by EDR, as it is expected, considering the radiation from resonating dipoles. The fields, induced by the radiation, apparently define peaking of P2 signal at $\lambda = 636$ nm that marks the maximal result of constructive interference. Subsequent drop of P2 signal at shorter wavelengths should be related to conversion to destructive interference between background radiation and fields, induced by radiation from EDRs, since the latter gradually switches its phase by π radians. In difference from resonance fields, background radiation experiences no phase switching and, therefore, finally becomes π radians different in phase with respect to resonance fields on the blue side of EDR. This fact defines mentioned above destructive interference between background radiation and fields induced by EDR that leads to zero probe signal in X-oriented gaps (point P2) at $\lambda = 625$ nm. Since gradual switching of the phase of P1 signal by π is almost completed at the wavelengths, corresponding to the π radians jump in P2 phase spectrum, this jump cannot be related to the resonance phenomenon. Instead, it is reasonable to suggest that the jump in P2 spectrum is the result of prevailing of background fields over decaying fields induced by resonance radiation on the blue side of EDR. It is obvious that at $\lambda < 625$ nm, decaying radiation from EDR becomes incapable of balancing the background radiation, so that the latter starts to control the phase of P2 signal.

Exemplified above approach to analyzing spectral changes of probe signal phases can be similarly employed for clarifying the nature of processes, defining the formation of Fano resonance at other probe locations.

VII. FANO RESONANCES AND INDUCED TRANSPARENCY

Conducted analysis of Fano resonances in MSs under study helped us to reveal the specifics of interference processes in these structures. In order to relate these processes to appearance of the EIT phenomenon, it is worth recalling the approaches, used in the first works on EIT.[1–3] Figure 14 shows a typical schematic, employed for explaining zero energy absorption at EIT in atomic

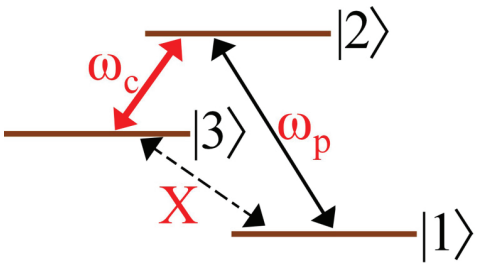

FIG. 14. Three level schematic used to explain the role of coupled transitions between states 3 and 2 for eliminating the energy absorption.

gases. The central idea was that no energy spending could be provided due to destructive interference between the competing transitions 1–2 and 3–2.

Thus, quantum interference was assumed capable of controlling the entire optical response, in particular, of eliminating the absorption and the refraction (linear susceptibility) at the resonant frequency. In such cases, from the side of observer, located in state 1, the situation could be seen as absence of any transitions between state 1 and state 3. The reality of such situations was in detail analyzed in Ref. 28.

Considering EIT in MSs under study, an analogy with the case of atomic gases could be seen in destructive interference between background/incident radiation and radiation from dipolar resonances, which was shown to be critical for the signals in point P2. In fact, for an observer, located in point P2, MS response at zero signal in the Fano lineshape will be seen as identical to the case with no background radiation and, so, with no presence of incident waves in the MS. In this case, the observer should not expect any absorption or refraction of incident waves, as well as their reflection (at zero susceptibility and zero index). Therefore, it seems logical to assume that at zero signal in the Fano lineshape in point P2, nothing prevents waves from transmitting without losses through MS and, so, the conditions for EIT could be realized.

It is worth pointing out here that the spectral distance between the positions of EDR and zero signal in Fano lineshape in point P2 is just a few nanometers at $\Delta = 275$ nm. Therefore, in S-parameter spectra, the EIT position appears almost indistinguishable from the EDR position. More accurate studies of EDR and EIT spectral positions at varying the Δ values are desired to additionally verify the character of correlation between two phenomena.

It could also be noticed that we did not observe EIT-like phenomena associated with magnetic dipolar resonances (MDRs). The reason for this could be seen in Fig. 3. As seen in the figure, in dense MSs, Q-factors of MDRs are very low. In sparse MSs, Q-factors of MDRs become higher, however, sparse MSs do not create conditions for superposition of fields required for the formation of Fano-resonances.

VIII. CONCLUSIONS

Numerical experiments with MSs, composed of identical cylindrical silicon nano-resonators, have shown that these structures can demonstrate full narrowband transparency for normally incident plane waves at the frequencies of EDRs. In MSs with square lattices, this EIT-like phenomenon has been observed only at the lattice constants in the range between 275 nm and 325 nm, i.e., in densely packed MSs.

The studies of electric field distributions in planar cross sections of MSs and of signal spectra from E-field probes placed in characteristic points of MS's unit cells helped us to identify physical processes, defining the specifics of Fano resonances observed at various probe locations. In particular, it was shown that Fano resonances, detected in the gaps between resonators, arranged along the E-field direction, were controlled by interference between background radiation and waves, radiated by resonance fields, formed inside DRs. Well known switching of the phase of resonance oscillations by π radians at the resonance frequency made this interference transforming from constructive to destructive at passing the resonance. Destructive interference provided suppression of background radiation and full MS transparency at the frequencies of zero signals in Fano lineshapes, registered at the locations described above. The wavelengths of spectral positions of the above zero signals were found to be about several nanometers shorter than the EDR wavelengths that created an illusion of coincidence of EIT and EDR effects.

ACKNOWLEDGMENTS

This work was supported by the National Science Foundation (NSF) under Award No. ECCS-1709991. The authors would like to thank Fatemeh Safari for her collaboration at performing microwave experiments.

DATA AVAILABILITY

The data that support the findings of this study are available from the corresponding author upon reasonable request.

REFERENCES

[1]O. A. Kocharovskaya and Y. I. Khanin, "Population trapping and coherent bleaching of a three-level medium by a periodic train of ultrashort pulses," Sov. Phys. JETP **63**(5), 945–950 (1986).
[2]K.-J. Boller, A. Imamoglu, and S. E. Harris, "Observation of electromagnetically induced transparency," Phys. Rev. Lett. **66**, 2593–2596 (1991).
[3]S. E. Harris, "Electromagnetically induced transparency," Phys. Today **50**(7), 36 (1997).
[4]N. Papasimakis, V. A. Fedotov, N. I. Zheludev, and S. L. Prosvirnin, "A metamaterial analog of electromagnetically induced transparency," Phys. Rev. Lett. **101**(25), 253903 (2008).
[5]S. Zhang, D. A. Genov, Y. Wang, M. Liu, and X. Zhang, "Plasmon-induced transparency in metamaterials," Phys. Rev. Lett. **101**, 047401 (2008).
[6]N. Papasimakis and N. I. Zheludev, "Metamaterial-induced transparency: Sharp Fano resonances and slow light," Opt. Photonics News **20**(10), 22–27 (2009).
[7]S.-Y. Chiam, R. Singh, C. Rockstuhl, F. Lederer, W. Zhang, and A. A. Bettiol1, "Analogue of electromagnetically induced transparency in a terahertz metamaterial," Phys. Rev. B **80**, 153103 (2009).
[8]Y. Yang, I. I. Kravchenko, D. P. Briggs, and J. Valentine, "All-dielectric metasurface analogue of electromagnetically induced transparency," Nat. Commun. **5**, 5753 (2014).

[9]B. Han, X. Li, C. Sui, J. Diao, X. Jing, and Z. Hong, "Analog of electromagnetically induced transparency in an E-shaped all-dielectric metasurface based on toroidal dipolar response," Opt. Mater. Express **8**(8), 2197 (2018).
[10]M. Qin, C. Pan, Y. Chen, Q. Ma, S. Liu, E. Wu, and B. Wu, "Electromagnetically induced transparency in all-dielectric U-shaped silicon metamaterials," Appl. Sci. **8**, 1799 (2018).
[11]L. Garrido Alzar, M. A. G. Martinez, and P. Nussenzveig, "Classical analog of electromagnetically induced transparency," Am. J. Phys. **70**, 37 (2002).
[12]S. Jamilan, G. Semouchkin, N. P. Gandji, and E. Semouchkina, "Specifics of scattering and radiation from sparse and dense dielectric meta-surfaces," J. Appl. Phys. **125**(16), 163106 (2019).
[13]S. Jamilan, G. Semouchkin, N. P. Gandji, and E. Semouchkina, "Electromagnetically induced transparency and lattice resonances in metasurfaces composed of silicon nanocylinders," in *AES 2019, Lisbon, Portugal, 24-26 July 2019* (Meta Publishing, 2019); available at https://metapublishing.org/index.php/MP/catalog/book/66.
[14]B. Luk'yanchuk, N. I. Zheludev, S. A. Maier, N. J. Halas, P. Nordlander, H. Giessen, and C. C. Tow, "The Fano resonance in plasmonic nanostructures and me," Nat. Mater. **9**(9), 707–715 (2010).
[15]R. Pant, S. Shakthi, and A. B. Yelikar, "Wideband excitation of Fano resonances and induced transparency by coherent interactions between Brillouin resonances," Sci. Rep. **8**, 9175 (2018).
[16]L. V. Hau, S. E. Harris, Z. Dutton, and C. H. Behroozi, "Light speed reduction to 17 metres per second in an ultracold atomic gas," Nature **6027**, 594 (1999).
[17]D. F. Phillips, A. Fleischhauer, A. Mair, R. L. Walsworth, and M. D. Lukin, "Storage of light in atomic vapor," Phys. Rev. Lett. **86**(5) 783–786 (2001).
[18]M. F. Yanik, W. Suh, Z. Wang and S. Fan, "Stopping light in a waveguide with an all-optical analog of electromagnetically induced transparency," Phys. Rev. Lett. **93**, 233903 (2004).
[19]R. S. Tucker, P.-C. Ku, and C. J. Chang-Hasnain, "Slow-light optical buffers: Capabilities and fundamental limitations," J. Lightwave Technol. **23**(12), 4046–4066 (2005).
[20]S. A. Schulz, A. A. Liles, and L. O'Faolain, "Tunable optical buffer through an analogue to electromagnetically induced transparency in coupled photonic crystal cavities," ACS Photonics **5**(5), 1827–1832 (2018).
[21]H. Schmidt and R. J. Ram, "All-optical wavelength converter and switch based on electromagnetically induced transparency," Appl. Phys. Lett. **76**, 3173 (2000).
[22]G. Sun, S. Peng, X. Zhang, and Y. Zhu, "Switchable electromagnetically induced transparency with toroidal mode in a graphene-loaded all-dielectric metasurface," Nanomaterials **10**(6), 1064, (2020).
[23]N. P. Gandji, G. Semouchkin, and E. Semouchkina, "Electromagnetic responses from planar arrays of dielectric nano-disks at overlapping dipolar resonances," in IEEE Research and Applications of Photonics in Defense Conference (RAPID) (IEEE, 2018).
[24]S. Jamilan, N. Gandji, G. Semouchkin, F. Safari, and E. Semouchkina, "Scattering from dielectric metasurfaces in optical and microwave ranges," IEEE Photonics J. **11**(3), 1–7 (2019).
[25]I. Staude, A. E. Miroshnichenko, M. Decker, N. T. Fofang, S. Liu, E. Gonzales, J. Dominguez, T. S. Luk, D. N. Neshev, I. Brener, and Y. Kivshar, "Tailoring directional scattering through magnetic and electric resonances in subwavelength silicon nanodisks," ACS Nano **7**(9), 7824 (2013).
[26]A. I. Kuznetsov, A. E. Miroshnichenko, M. L. Brongersma, Y. S. Kivshar, and B. Luk'yanchuk, "Optically resonant dielectric nanostructures," Science **354**, aag2472 (2016).
[27]S. Jamilan and E. Semouchkina, "Lattice resonances in metasurfaces composed of silicon nano-cylinders," in 14th Intern. Congress on Artificial Materials for Novel Wave Phenomena—Metamaterials, NY (IEEE, 2020).
[28]M. Fleischhauer, A. Imamoglu, and J. P. Marangos, "Electromagnetically induced transparency: Optics in coherent media," Rev. Modern Phys. **77**, 633 (2005).